International Journal of Engineering, Mathematical and Physical Sciences
ISSN: 2517-9934
Vol:8, No:3, 2014

Production of Size-Selected Tin Nanoclusters for Device Applications

Ahmad I. Ayesh

***Abstract*—**This work reports on the fabrication of tin nanoclusters by sputtering and inert-gas condensation inside an ultra-high vacuum compatible system. This technique allows to fine tune the size and yield of nanoclusters by controlling the nanocluster source parameters. The produced nanoclusters are deposited on SiO_2/Si substrate with pre-formed electrical electrodes to produce a nanocluster device. Those devices can be potentially used for gas sensor applications.

***Keywords*—**Tin, nanoclusters, inert-gas condensation.

I. Introduction

ATOMIC nanoclusters are aggregates of atom that are nanometer in size, and their physical and chemical properties are different from their bulk equivalents. Upon reducing a material size into nanosize, the number of surface atoms becomes large compared with the total number of atoms inside the material. The surface atoms of a nanocluster have fewer nearest neighbors, thus, less strongly bound. This has great impact on the ability of nanoclusters to interact with external materials. Therefore, they can be utilized efficiently for gas sensing applications [1]-[5]. Tin oxide (SnO_2) nanoclusters are of the most used nanoclusters for gas sensor applications due to their supreme performances in terms of sensitivity and stability compared to other nanoclusters [6], [7].

The objective of this work is to fabricate tin (Sn) nanoclusters by sputtering and inert gas condensation, and investigate the effect of nanocluster source parameters on nanocluster size and yield. This technique of nanocluster fabrication has many advantages such as [8]-[10]: the high purity of the produced nanoclusters; size selection of nanoclusters is possible using a suitable mass filter since the produced nanoclusters are charged; the produced nanoclusters are of narrow size distribution; the size of nanoclusters can be tuned "easily" within a range of sizes correspond to the source design by controlling the source parameters (as discussed below); the composition of the produced nanoclusters is controlled by controlling the composition of the target material; the produced nanoclusters can be self-assemble directly on a substrate to create a device; the coverage of the deposited nanoclusters on the substrate and thus the sensitive layer thickness is controllable by controlling the deposition time; and the technique could be used on an industrial scale.

Ahmad I. Ayesh is in the Department of Physics, United Arab Emirates University, Al Ain, United Arab Emirates, P.O.Box 15551 (e-mail: ayesh@uaeu.ac.ae).

II. Experimental

Tin nanoclusters were produced using a magnetron sputtering plasma and inert-gas condensation source inside an ultra-high vacuum (UHV) compatible system [8], [9]. The system consists of two chambers: the source and main chambers, which were evacuated to a base pressure of ~10^{-8} mbar before nanocluster production. The dc magnetron type discharge was utilized to generate nanoclusters from a Sn target using a discharge power (P) of 15 W unless it is stated otherwise. Argon (Ar) gas was used to generate the plasma, sputter the material from a 99.995% purity Sn target that was fixed on the magnetron sputter head, and aggregate Sn nanoclusters from the sputtered material. A MKS Instruments mass flow controller was used to control Ar flow rate (f) in the range of 0 – 100sccm (sccm stands for standard cubic centimeter per minute). The magnetron gun was mounted on a motorized linear translator, enabling the aggregation length (L) to be varied by up to 100mm. The aggregation length is the distance from the surface of the sputtering target to the source exit nozzle. Ar gas inside the source chamber created a pressure difference between the source and the main chambers that forced the nanoclusters to travel through the quadrupole mass filter (QMF) and then to the main chamber. Ar gas was pumped away from the source and main chambers using two turbo pumps (for details see [8], [9]).

The QMF was used to measure the nanocluster size distribution before its deposition inside the main chamber, with a maximum resolution U/V = 0.168. The quadrupole mass filter was operated by connecting one pair of rods to a potential (U+Vcosωt) and the other to -(U+Vcosωt), where U is a dc voltage and Vcosωt is an ac voltage [11]. Assuming spherical nanoclusters, the size of a nanocluster (D) refers to its diameter. A grid located at the exit of the mass filter – Faraday cup– was used to measure the electric current signal for ionized nanoclusters of each selected size, and the current was measured by a picoammeter. The area under a size distribution curve refers to the number of nanoclusters generated inside the source and detected using the Faraday cup. Thus, the area under a size distribution curve is defined in this context as the "*nanocluster yield*".

A directed nanocluster beam is formed once the nanoclusters leave the QMF. The nanoclusters deposition rate is measured using a quartz crystal monitor (QCM). The QCM is fixed on a motorized linear translator that enables driving the QCM in front of the exit nozzle, check the deposition rate, and then drive it back away from the beam path. The position of the liner translators holding the magnetron gun, QCM, and sample holder can be varied without venting the system.

The produced nanoclusters were used to fabricate nanocluster devices. The nanoclusters were deposited on a SiO_2/Si substrates fixed on a sample holder which is mounted on a vertical motorized linear translator inside the main chamber. The substrate has a pair of parallel Au/NiCr electrical electrodes (thickness ~50nm) deposited by thermal evaporation. The separation between the electrodes is 50µm. Electrical measurements were subsequently conducted for the devices using a Keithley236 source measuring unit.

III. Results

The performance of the QMF was investigated initially to select a suitable value of U/V. Fig. 1 (a) shows nanocluster size distributions generated at different U/V values. The average nanocluster size as well as the area under each size distribution curves were calculated and shown in Fig. 1 (b). Figs. 1 (a) and (b) show that increasing U/V keeps the average nanocluster size constant and decreases nanocluster yield. The main features of the size distribution remain the same. U/V of 0.12 was found to produce a reasonable yield of nanoclusters with suitable resolution, thus, it is used for this work.

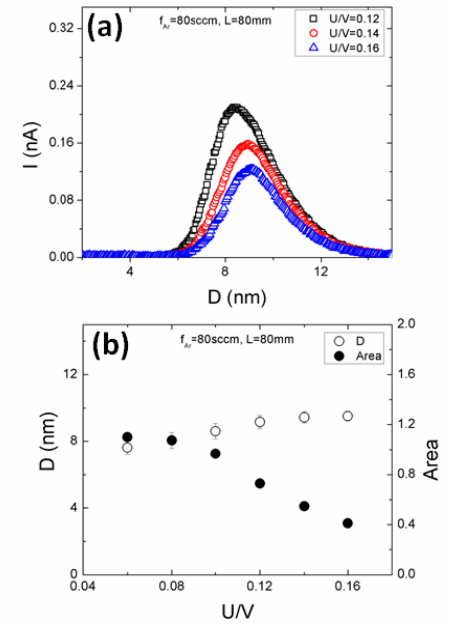

Fig. 1 (a) Sn nanocluster size distribution at different U/V values (b) The variation of nanocluster size and yield as a function of U/V

Fig. 2 (a) shows the size distributions of Sn nanoclusters produced at L = 80mm. The figure shows that increasing f produces a clear effect on nanocluster average size and yield. The variation of nanocluster average size and yield with f is shown in Fig. 2 (b). The figure shows that increasing f increases D.

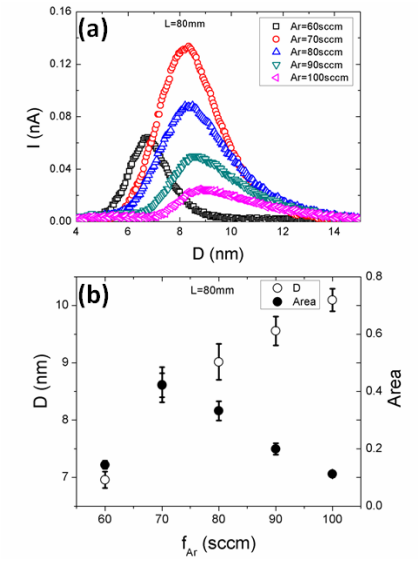

Fig. 2 (a) Sn nanocluster size distribution at different inert-gas flow rate values (b) The variation of nanocluster size and yield as a function of inert-gas flow rate

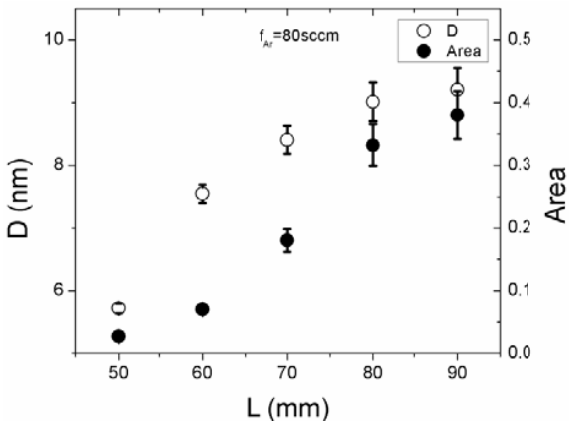

Fig. 3 The variation of nanocluster size and yield as a function of aggregation length

However, nanocluster yield increases and then decreases with f.

The variation of average nanocluster size and yield with aggregation length is shown in Fig. 3. The figure reveals that increasing the aggregation length increases the average nanocluster size as well as the yield. Fig. 4 shows the dependence of average nanocluster size and yield on the sputtering discharge power. The figure shows that both size and yield exhibit similar behavior with P except at high discharge power.

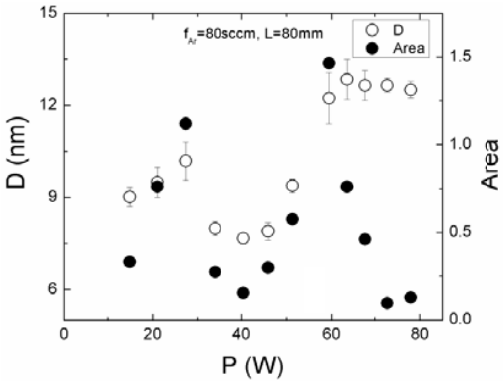

Fig. 4 The variation of nanocluster size and yield as a function of sputtering discharge power

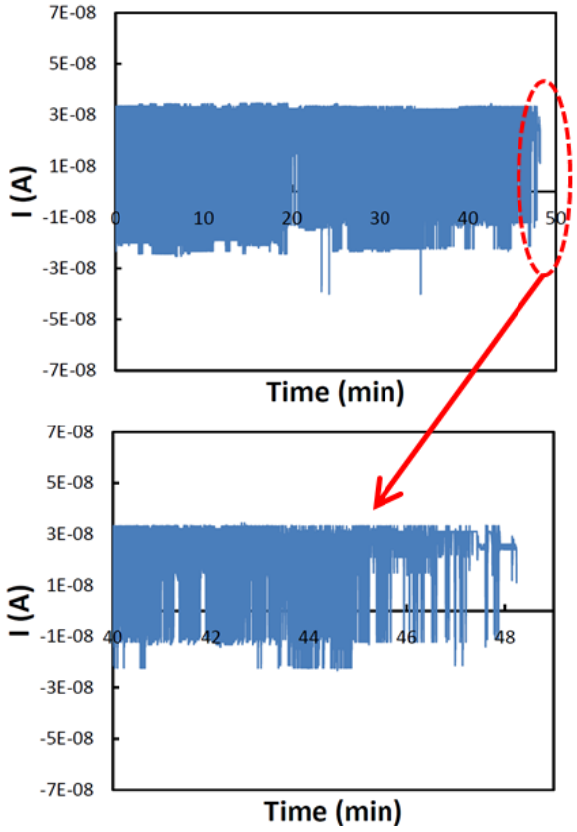

Fig. 5 The electric current through a Sn nanocluster device using V = 0.1 V

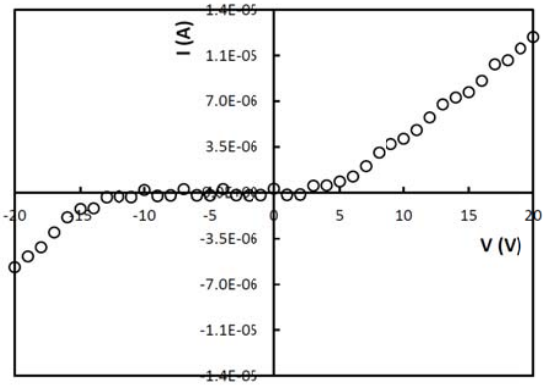

Fig. 6 Current-voltage characteristics of a Sn nanocluster device

To fabricate a nanocluster device, nanoclusters are deposited on the substrate. Simultaneously, a constant voltage of 0.1 V was applied across the Au/NiCr electrodes and the electrical current was measured (using a Keithley 236 source measuring unit). Initially the electrical current was too small and fluctuating between negative and positive values as shown in Fig. 5. This indicates that nanoclusters on the substrate are discontinuous. The fluctuation of the current between positive and negative values result from nanoclusters that land on the electrical electrodes and is due to the fact that the majority of nanoclusters produced by sputtering are charged (either positive or negative charges). Once a continuous network of nanoclusters is formed, the electrical current becomes positive only (see Fig. 5), thus, nanocluster deposition is stopped suddenly using an automatic shutter. Fig. 6 shows the current-voltage (I(V)) characteristics of a Sn nanocluster device. The I(V) curve reveals non-linear behavior. It should be noted here that the nanoclusters used to fabricate the device are ~ 12nm in size and formed using P = 60W, f = 80sccm, and L = 80mm (see Fig. 4).

IV. Discussion

The variation of nanocluster size with f can be explained in terms of nanocluster formation mechanisms. Two types of collisions might be involved in nanocluster production: i) three–body collision in which two sputtered atoms lose their excess kinetic energy by colliding with an Ar atom; and ii) two–body collisions in which nanocluster growth occurs via nanocluster–atom (atomic condensation) and nanocluster–nanocluster collisions [12]-[15]. Nanocluster seeds are initiated through three–body collisions due to cooling of the sputtered atoms by Ar atoms. The probability of the three–body collision is determined by the density of atomic vapor, and the nucleation and growth times. Thus, for the three–body collision mechanism, nanocluster size is expected to decrease as f increases because of the high drift velocity of the material within the growth region (i.e., the nucleation and growth time decreases) [8]. Herein, the number of metal atoms (or small nanoclusters) that can combine with a nanocluster decreases as f increases, thus, nanocluster growth is reduced [16]. The nanoclusters grow further by the two-body collision

mechanism [17]. When the two–body collision mechanism is dominant, larger nanoclusters are produced [8], [17]. As f increases, the mean–free–path decreases, and this in turn increases the probability of the two–body collisions which allows further nanocluster–atom and nanocluster–nanocluster collisions [16]. Therefore, the increase of D with f for Sn indicates the dominance of the two–body collision mechanism for Sn nanocluster production.

The decrease in the nanocluster yield with f, observed in Fig. 2 (b), is a result of consuming the nanoclusters to produce larger nanoclusters. This argument is consistent with the variation of D with f, where the increase in D with f is mainly due to nanocluster–nanocluster (two–body) collision mechanism. The small number of produced nanoclusters at low f, observed in Fig. 2 (b) could be the result of low nanocluster yield of Sn at the lowest possible f. Nanocluster growth via the two–body collision mechanism involves either nanocluster–nanocluster collisions, or/and nanocluster–atom collisions. The probability of these collisions governs the number of produced nanoclusters [15]. The nanocluster yield is expected to increase with f if the nanocluster–atom collision is dominant and more condensation occurs. Nevertheless, the nanocluster yield is likely to decrease with f if the nanocluster–nanocluster collision is dominant because nanoclusters are expended to produce larger ones [17]. Therefore, the maximum yield at f = 70sccm in Fig. 2 (b) indicates that the nucleation and growth are dominated by two–body collision mechanism (nanocluster–atom). The small number of nanoclusters at low f indicates that their production is determined mainly by the two–body (nanocluster–nanocluster) collision mechanism as evident in Fig. 2. Thus, nanoclusters are consumed to generate larger ones. Nevertheless, the low yield at high f might be assigned to a larger contribution of the nanocluster–nanocluster collision compared to the nanocluster–atom collision which could be attributed to the larger mass of Sn atoms (smaller mean-free-path).

The direct increase of D with L, illustrated in Fig. 3 can be understood in terms of nanocluster nucleation and growth time. Increasing the aggregation length causes the nanoclusters to remain longer within the aggregation region, which in turn supports nanocluster growth and yield.

Optimizing the sputtering discharge power is crucial for producing nanoclusters with a required size and adequate yield. An insufficient discharge power would not produce enough self-bias on the target, thus, nanoclusters cannot be detected. Low yield of nanoclusters were produced at lower or higher discharge power. Experimental studies showed that nanoclusters can be produced within an optimum range of sputtering discharge power [12]. At low sputtering power insufficient self-bias on the target would produce a tiny number of small nanoclusters. On the other hand, the plasma becomes unstable when P is too high, which causes an intermittent in nanocluster production [12]. As a result, the amount of sputtered material decreases, which in turn decreases the probability of material collision, and thus, nanocluster yield.

The non-linear I(V) characteristics shown in Fig. 6 indicates that Coulomb blockade dictate the transport properties of the nanocluster network between the adjacent nanoclusters, or nanocluster film with the electrodes [18]. This behavior has been observed previously for other nanocluster and nanorod systems [19].

V. Conclusion

In conclusion, tin nanoclusters were formed by sputtering and inert-gas condensation inside an ultra-high compatible vacuum system. This technique enabled fine tune of nanocluster size and yield by controlling the nanocluster source parameters. The produced nanoclusters were used to fabricate nanocluster devices. Those devices were found to exhibit non-linear I(V) characteristics, and they have a potential to be used for gas sensor devices.

References

[1] P. Mazzoldi, G.W. Arnold, G. Battaglin, F. Gonella and R.F. Haglund: Metal nanocluster formation by ion implantation in silicate glasses. J. Nonlin. Opt. Phys. Mater. 5, 1996, p. 285.

[2] A. Martucci, M. De Nuntis, A. Ribaudo, M. Guglielmi, S. Padovani, F. Enrichi, G. Mattei, P. Mazzoldi, C. Sada, E. Trave, G. Battaglin, F. Gonella, E. Borsella, M. Falconieri, M. Patrini and J. Fick: Silver-sensitized erbium-doped ion-exchanged sol-gel waveguides. Appl. Phys. A 80, 2005, p. 557.

[3] Karvianto and G.M. Chow: The effects of surface and surface coatings on fluorescence properties of hollow NaYF(4):Yb,Erupconversion nanoparticles. J. Mater. Res. 14, 2011, p. 70.

[4] C. de JuliánFernández, C. Sangregorio, G. Mattei, G. De, A. Saber, S. Lo Russo, G. Battaglin, M. Catalano, E. Cattaruzza, F. Gonella, D. Gatteschi and P. Mazzoldi: Structure and magnetic properties of alloy-based nanoparticles silica composites prepared by ion-implantation and sol-gel techniques. Mater. Sci. Eng. C 15, 2001, p. 59.

[5] C. de JuliánFernández, G. Mattei, C. Maurizio, E. Cattaruzza, S. Padovani, G. Battaglin, F. Gonella, F. D'Acapito and P. Mazzoldi: Magnetic properties of Co-Cu nanoparticles dispersed in silica matrix. J. Magn. Magn. Mater. 187, 2005, p. 290.

[6] V. Aroutiounian: Metal oxide hydrogen, oxygen, and carbon monoxide sensors for hydrogen setups and cells. International Journal of Hydrogen Energy 32, 2007, p. 1145.

[7] P. Bonzi, L.E. Depero, F. Parmigiani, C. Perego, G. Sberveglieri, and G. Quattroni: Formation and structure of tin-iron oxide thin film CO sensors. J. Mater. Res. 9, 1994, p. 1250.

[8] A. I. Ayesh, N. Qamhieh, H. Ghamlouche, S. Thaker, and M. EL-Shaer: Fabrication of size-selected Pd nanoclusters using a magnetron plasma sputtering source. J. Appl. Phys. 107, 2010, p. 034317.

[9] A. I. Ayesh, S. Thaker, N. Qamhieh, and H. Ghamlouche: Size-controlled Pd nanocluster grown by plasma gas-condensation method. J. Nanopart. Res. 13, 2011, p. 1125.

[10] A. I. Ayesh, N. Qamhieh, S. T. Mahmoud, and H. Alawadhi: Production of size-selected CuxSn1-x nanoclusters. Advanced Materials Research 295-297, 2011, pp. 70-73.

[11] P. H. Dawson: Quadrupole Mass Spectrometry and its Applications, Elsevier Press, New York (1976).

[12] S. Pratontep, S. J. Carroll, C. Xirouchaki, M. Streun, and R. E. Palmer: Size-selected cluster beam source based on radio frequency magnetron plasma sputtering and gas condensation. Rev. Sci. Instrum. 76, 2005, p. 045103.

[13] E. L. Knuth: Size correlations for condensation clusters produced in free-jet expansions. J. Chem. Phys. 107, 1997, p. 9125.

[14] A. N. Banerjee, R. Krishna, and B. Das: Size controlled deposition of Cu and Si nano-clusters by an ultra-high vacuum sputtering gas aggregation technique. Appl. Phys. A 90, 2008, p. 299.

[15] H. Haberland, Nanoclusters of Atoms and Molecules, Springer, Berlin, 1995.

[16] S. Yamamuro, K. Sumiyama, W. Sakurai, and K. Suzuki, Cr cluster deposition by plasma-gas-condensation method. Supramolecular Science 5, 1998, p. 239.
[17] T. Hihara and K. Sumiyama: Formation and size control of a Ni cluster by plasma gas condensation. J. Appl. Phys. 84, 1998, p. 5270.
[18] A. I. Ayesh, 'Electronic transport in Pd nanocluster devices', Appl. Phys. Lett. 98, 2011, p. 133108.
[19] B. Ozturk, C. Blackledge, B. N. Flanders, and D. Grischkowsky, Appl. Phys. Lett. 88, 2006, p. 073108.